Nuclear Science and Techniques (2023) 34:85
https://doi.org/10.1007/s41365-023-01243-x

Investigation of the level spectra of nuclei in the northeast region of doubly magic ^{40}Ca with intruder orbit $g_{9/2}$

Jin-Zhong Han[1] · Shuai Xu[1] · Amir Jalili[2,3] · Han-Kui Wang[2,4]

Received: 6 March 2023 / Revised: 12 April 2023 / Accepted: 21 April 2023 / Published online: 21 June 2023

Abstract

This study utilizes large-scale shell model calculations with the extended pairing and multipole–multipole force model (EPQQM) to investigate low-lying states in the nuclei of ^{42}Ca, ^{42}Sc, and $^{42-44}$Ti. The model space in this study includes the *fp* shell as well as the intruder $g_{9/2}$ orbit, which accurately reproduces the positive parity levels observed in the aforementioned nuclei and predicts high energy states with negative parity coupled with the intruder $g_{9/2}$. The study further predicts two different configurations in ^{43}Ti at around 6 MeV, specifically $\pi f_{7/2}^2 \nu g_{9/2}$ and $\pi f_{7/2} g_{9/2} \nu f_{7/2}$, both of which involve the intruder orbit $g_{9/2}$. The levels coupled with the intruder $g_{9/2}$ in ^{44}Ti are predicted to lie between 7 and 11 MeV. The inclusion of the intruder orbit $g_{9/2}$ is crucial for the exploration of high energy states in the northeast region of the doubly magic nucleus ^{40}Ca.

Keywords Shell model · Doubly magic · Level structure

1 Introduction

The study of nuclei in the northeast of the doubly magic nucleus ^{40}Ca is a topic of great interest in both experimental and theoretical nuclear structure research. In pioneering experimental research, the lifetimes of higher-lying positive parity levels have been determined with limited precision [1–3]. Subsequently, negative parity states have been investigated, ultimately determining the 4^- [4]. The negative parity level 3^- was first confirmed by a preliminary lifetime analysis in a conference proceeding in 2011 [5]. More recently, the lifetimes of excited states have been determined in ^{44}Ti with high accuracy, using the recoil distance Doppler-shift method [6, 7]. Some of the recent advancements in both experimental and theoretical research regarding 2p decay, including technical innovations for measuring nucleon-nucleon correlations as well as developments in the models used to connect the structural aspects of nuclei with their corresponding decay properties, are presented in Ref. [8]. In the IMS experiments, charge resolution provides crucial information for the particle identification of ion pairs [9]. These newly proposed models were used to predict the cross-sections of ERIs produced in projectile fragmentation reactions of 140 MeV/u ^{78,86}Kr/^{58,64}Ni/^{40,48}Ca + ^{9}Be [10].

The half-life of β-decay and β-delayed neutron emission (βn) are crucial parameters in the advancement of basic science and industrial applications, including nuclear physics and nuclear energy, according to theoretical considerations [11]. The excited states of Ti isotopes have been studied microscopically within a single j-shell formalism [12]. A comparative study has been performed in *pf* shell nuclei

Research at ZSTU is supported by the National Natural Science Foundation of China (No. U2267205). Research at ZKNU is supported by the High-level Talents Research and Startup Foundation Projects for Doctors of Zhoukou Normal University (No. ZKNUC2021006) and Scientific research projects of universities in Henan Province (No. 23A140027).

✉ Han-Kui Wang
whk2007@163.com

Jin-Zhong Han
Hanjinzhong@zknu.edu.cn

[1] School of Physics and Telecommunication Engineering, Zhoukou Normal University, Zhoukou 466000, China

[2] Department of Physics, Zhejiang SCI-TECH University, Hangzhou 310018, China

[3] School of Physics, Nankai University, Tianjin 300071, China

[4] School of Physics and Astronomy, Shanghai Jiao Tong University, Shanghai 200240, China

using the cranked Nilsson-Strutinsky model and the spherical shell model [13]. Over the decades, various models have been developed to study the spectroscopic properties of nuclei such as the large-scale spherical shell model calculations, which have demonstrated excellent agreement with observed data. One such model is the SDPFMU interaction [14], which is based on existing interactions and uses valence shells *sd* and *pf*. For instance, it is based on the USD interaction [15] and GXPF1 [16] for the *sd* and *pf* shells, respectively. The monopole interactions are based on the SDPF-M model [17], and the monopole- and quadrupole-pairing matrix elements are replaced with KB3 [18]. Another model, the EPQQM (expanded pairing, quadrupole–quadrupole, and multipole force with monopole corrections) model, has been found to work efficiently in various mass regions, such as the proton-rich *pf* shell [19], the $pf_{5/2}g_{9/2}$ shell [20], the neutron-rich *fpg* shell [21], and the $sd-pf$ shell [22]. This model has been particularly successful in explaining both the low-lying levels and the high core excitations in the heavy, neutron-rich region near $A = 130$ [23–25], in addition to confirming the persistence of the $N = 82$ shell closure and effectively describing the ground state inversion in ^{129}Cd driven by monopole interaction between protons and neutrons [26, 27].

The intruder orbit $g_{9/2}$ is crucial between the *df* and *pf* shells. Intruder states refer to those states that lie outside the traditional or expected valence configurations. These states can have a significant impact on the structure of a nucleus. For example, they can lead to ground state or low-lying excited state inversions, where the ordering of the energy levels is different from the traditional shell model predictions. Intruder states can also affect various properties of nuclei, including their energy levels and ratios. These states are particularly significant in comprehending the evolution of nuclear structure as the number of neutrons or protons changes. In the present study, the EPQQM model, which includes the intruder $g_{9/2}$ orbit in the model space, is used to investigate the energy levels of nuclei in the northeast of ^{40}Ca. The inclusion of the intruder orbit allows for a more complete description of the positive parity levels and the high energy states of negative parity levels in these nuclei.

In this model, the predicted energy levels are rigorously compared with experimental data to validate and refine its accuracy. This study highlights the importance of considering intruder states in the analysis of nuclear structure and the need for experimental measurements in validating model predictions. Intruder states can also be related to the phenomenon of shape coexistence, which is the existence of different shapes in the ground state of a nucleus, due to the mixing of different configurations [28, 29]. This phenomenon is observed in various nuclei, and the inclusion of intruder states in the model space allows for a more complete description of the observed shape coexistence. Therefore, the inclusion of intruder states in nuclear models is vital for gaining a deeper understanding of the evolution of nuclear shape, the phenomenon of shape coexistence, and the potential emergence of new magic numbers.

In this work, the EPQQM model in the model space of the *pf* shell, including the intruder $g_{9/2}$ orbit, is applied to investigate the energy levels of nuclei in the northeast of ^{40}Ca. The positive parity levels and intruder states in ^{42}Ca, ^{42}Sc, and ^{42}Ti are efficiently described by the EPQQM interaction. The nuclei ^{43}Ti and ^{44}Ti are also examined by comparing them with experimental data [30], serving as an additional means to further test the two-body strengths in nuclear models. The calculations for the nuclei ^{43}Ti and ^{44}Ti are performed using the shell model code NUSHELLX@MSU [31]. The SDPFUM interaction is utilized to explore the cross-shell excitation originating from the $d_{5/2}$ orbit under $Z = 20$ ($N = 20$). Additionally, the GXPF1A interaction [16] is employed for comparison purposes to study the energy levels within the *pf* shell.

2 Theoretical framework

The results obtained from the study of nuclei in the northeast region of the doubly magic nucleus ^{40}Ca have significant implications for nuclear physics research. In particular, the inclusion of intruder states, such as the $g_{9/2}$ orbit, has been demonstrated to be critical for a comprehensive understanding of nuclear structure. This study provides additional support for the utilization of the EPQQM model in describing the energy levels of nuclei, particularly focusing on the northeast region of ^{40}Ca.

Theoretical models are essential in nuclear physics as they provide valuable insights into the properties of nuclei that are difficult to measure directly through experiments. The SDPFMU and EPQQM models, in particular, have shown promising results in various mass regions, including the $sd-pf$, proton-rich *pf* shell, and heavy neutron-rich region near $A = 130$. These models can accurately predict the properties of nuclei, such as their energy levels and ratios, as well as describe shape coexistence and ground state inversions. They have helped recognize the importance of intruder states in the evolution of nuclear structure.

Although theoretical models are powerful tools, their predictions must be validated through experimental measurements to ensure their full verification. The results of this this study can guide future experimental investigations in the northeast region of ^{40}Ca, such as the determination of the lifetimes of higher-lying positive parity levels with greater precision. The combination of experimental and theoretical approaches is crucial for advancing our understanding of nuclear structure and the fundamental properties of matter.

2.1 Hamiltonian

In the proton–neutron (*pn*) representation, the present Hamiltonian is composed of the pairing-plus-multipole force and the monopole corrections:

$$\begin{aligned} H &= H_{\rm sp} + H_{P_0} + H_{P_2} + H_{QQ} + H_{OO} + H_{HH} + H_{\rm mc} \\ &= \sum_{\alpha,i} \varepsilon^i_a c^\dagger_{\alpha,i} c_{\alpha,i} - \frac{1}{2} \sum_{J=0,2} \sum_{ii'} g_{J,ii'} \sum_M P^\dagger_{JM,ii'} P_{JM,ii'} \\ &\quad - \frac{1}{2} \sum_{ii'} \frac{\chi_{2,ii'}}{b^4} \sum_M : Q^\dagger_{2M,ii'} Q_{2M,ii'} : \\ &\quad - \frac{1}{2} \sum_{ii'} \frac{\chi_{3,ii'}}{b^6} \sum_M : O^\dagger_{3M,ii'} O_{3M,ii'} : \\ &\quad - \frac{1}{2} \sum_{ii'} \frac{\chi_{4,ii'}}{b^8} \sum_M : H^\dagger_{4M,ii'} H_{4M,ii'} : \\ &\quad + \sum_{a\le c,ii'} k_{\rm mc}(ia,i'c) \sum_{JM} A^\dagger_{JM}(ia,i'c) A_{JM}(ia,i'c). \end{aligned} \tag{1}$$

This effective interaction (1) includes the single-particle Hamiltonian ($H_{\rm sp}$), the $J=0$ and $J=2$ pairing ($P^\dagger_0 P_0$ and $P^\dagger_2 P_2$), the quadrupole–quadrupole ($Q^\dagger Q$), the octupole–octupole ($O^\dagger O$), the hexadecapole–hexadecapole ($H^\dagger H$) terms, and the monopole corrections ($H_{\rm mc}$). In the *pn* representation, $P^\dagger_{JM,ii'}$ and $A^\dagger_{JM}(ia,i'c)$ are the pair operators, while $Q^\dagger_{2M,ii'}$, $O^\dagger_{3M,ii'}$, and $H^\dagger_{4M,ii'}$ are the quadrupole, octupole, and hexadecapole operators, in which i (i') are indices for protons (neutrons). The parameters $g_{J,ii'}$, $\chi_{2,ii'}$, $\chi_{3,ii'}$, $\chi_{4,ii'}$, and $k_{\rm mc}(ia,i'c)$ are the corresponding force strengths, and b is the harmonic-oscillator range parameter. The two-body force strengths suited for the present model space are listed in Table 1.

2.2 Model space

In addition to the Hamiltonian, the choice of model spaces with single-particle energies are crucial for shell model calculations. In this work, the model space for protons (neutrons) consists of all the *pf* shell orbits ($1f_{7/2}$, $1f_{5/2}$, $2p_{1/2}$, $2p_{3/2}$) with frozen core ^{40}Ca. Further, an intruder state, the $1g_{9/2}$ orbit is added to study high energy levels. The low-lying levels in ^{41}Ca (^{41}Sc) are selected as neutron (proton) single-particle states in this model space to obtain single-particle energies. Marking $\varepsilon^\pi_{f7/2}$ as the single-particle energy (SPE) of the ground state $7/2^-$ in ^{41}Sc, π denoting proton (ν neutron), we obtain SPE as the difference in binding energies (BE) of ^{41}Sc and ^{40}Ca,

$$\varepsilon^\pi_{f7/2} = BE(^{41}\text{Sc}) - BE(^{40}\text{Ca}) = -1.089 \text{ MeV}. \tag{2}$$

The other proton SPE in ^{41}Sc can be obtained by adding this value $\epsilon^\pi_{f7/2} = -1.089$ MeV to the excited energies. Thus, all SPEs are obtained as follows (MeV):

$$\begin{aligned} &\varepsilon^\pi_{f7/2} = -1.089\,, \quad \varepsilon^\nu_{f7/2} = -8.387\,, \\ &\varepsilon^\pi_{p3/2} = 0.627\,, \quad \varepsilon^\nu_{p3/2} = -6.444\,, \\ &\varepsilon^\pi_{f5/2} = 1.499\,, \quad \varepsilon^\nu_{f5/2} = -5.811\,, \\ &\varepsilon^\pi_{p1/2} = 2.376\,, \quad \varepsilon^\nu_{p1/2} = -4.773\,, \\ &\varepsilon^\pi_{g9/2} = 3.425\,, \quad \varepsilon^\nu_{g9/2} = -3.936\,. \end{aligned} \tag{3}$$

For these neutron SPEs, the excited energies are taken as 0, 1.943, 2.576, 3.614, and 4.451 MeV from $7/2^-$, $3/2^-$, $5/2^-$, $3/2^-$, and $9/2^+$ levels in ^{41}Ca. For proton SPEs, they are 0, 1.716, 2.588, 3.465, and 4.514 MeV from $7/2^-$, $3/2^-$, $5/2^-$, $1/2^-$, and $9/2^+$ levels in ^{41}Sc.

2.3 Monopole corrections

In the present Hamiltonian, the monopole corrections can be investigated as follows:

$$Mc = k_{\rm mc}(ia,i'c) \sum_{JM} A^\dagger_{JM}(ia,i'c) A_{JM}(ia,i'c)\,. \tag{4}$$

Here $A^\dagger_{JM}(ia,i'c)$ and A_{JM} represent the pair operators, and $k_{\rm mc}$ is the monopole force strength. Monopole correction terms should consider corresponding data. Note that the maximum multiplet is $J=8$ coupled by the configuration $1f_{7/2}1g_{9/2}$. The datum 8^- at 6.408 MeV in ^{42}Ca is selected to determine the force strength of monopole correction between neutron orbits $1f_{7/2}$ and $1g_{9/2}$. There is no datum 8^- in ^{42}Ti; therefore, the force strength between proton orbits $1f_{7/2}$ and $1g_{9/2}$ refers to the value in ^{42}Ca.

$$\begin{aligned} Mc1 &\equiv k_{\rm mc}(\nu f_{7/2}, \nu g_{9/2}) = -1.10\text{MeV}, \\ Mc2 &\equiv k_{\rm mc}(\pi f_{7/2}, \pi g_{9/2}) = -1.10\text{MeV}. \end{aligned} \tag{5}$$

Owing to missing three-body contributions in the Hamiltonians derived from realistic two-body potentials [32, 33], monopole corrections become necessary for two-body interactions [34]. The extended pairing-plus-multipole–multipole force (EPQQM model) is advantageous in employing monopole correction (Mc) terms [35]. Monopole-driven shell evolutions are discussed with different effects of tensor forces in Ref. [36]. Monopole interactions are critical in

Table 1 Two-body force strengths (in MeV) used in the present calculation

ii'	$g_{0,ii'}$	$g_{2,ii'}$	$\chi_{2,ii'}$	$\chi_{3,ii'}$	$\chi_{4,ii'}$
pp	0.450	0.470	− 0.107	0.075	0.0010
nn	0.422	0.449	0	0.075	0.00010
pn	0	0	0.256	0	0.0009

shifting the spherical shell model to account for the non-conventional shell evolution observed in neutron-rich nuclei. Experimental studies have shown that the monopole interaction between the neutron orbits $h_{11/2}$ and $d_{3/2}$ provides an effective description of ground state inversions observed in isotopes ranging from ^{130}In(^{129}Cd) to ^{128}In(^{127}Cd) [37]. The energy gap of the neutron $N = 82$ can be modified by using a monopole term between $h_{11/2}$ and $f_{7/2}$. Experimental confirmation has validated the inverse low-lying levels of ^{129}Cd predicted by the monopole effect between $g_{9/2}$ and $h_{11/2}$. Monopole corrections have recently helped in constructing a new Hamiltonian above ^{132}Sn with core excitations and an intruder orbit $i_{13/2}$.

3 Results and discussions

In this part, structure analysis is carried out for ^{42}Ti, ^{42}Ca, ^{42}Sc, and ^{43,44}Ti with EPQQM, GXPF1A, and SDPFMU effective interactions. This work includes intruder states involving the $g_{9/2}$ orbit, with no restriction on the *pf* shell and $g_{9/2}$ orbit. The GXPF1A effective interaction has proven to be highly effective in the *pf* shell, and its results serve as a valuable benchmark for comparison. The SDPFMU interaction is applied to study the proton (neutron) core excitations across the $Z = 20$ ($N = 20$) energy gap, and one proton (neutron) core excitation is allowed across the $Z = 20$ ($N = 20$) shell gap from $d_{5/2}$ in *sd* shell.

3.1 ^{42}Ca

The $g_{9/2}$ orbit plays a crucial role in the energy spectrum of ^{42}Ca. Being an intruder orbit, it lies outside the traditional valence shell configuration of ^{40}Ca, which is composed of the *pf* shell. By including the $g_{9/2}$ orbit in the model space, additional degrees of freedom for nucleons are introduced, leading to new configurations and the possibility of new quantum numbers.

^{42}Ca, as a stable nucleus, exhibits a rich spectrum of excited states up to 11 MeV and spins up to $J = 12$. Only positive parity levels can be coupled with two valence nucleons in the *pf* shell, with the highest spin $J = 6$, resulting from the configuration coupling. However, negative parity levels arise from two distinct sources: cross-shell excitations or coupling with the intruder orbit $g_{9/2}$. In this study, we employ the EPQQM interaction to discuss levels coupled by the intruder orbit $g_{9/2}$ and the SDPFMU interaction to explore cross-shell excitations.

The determination of pairing and multipole force strengths in the neutron model space is facilitated by studying the low-lying states of ^{42}Ca. Figure 1 depicts a comparison between the experimental data for ^{42}Ca and shell

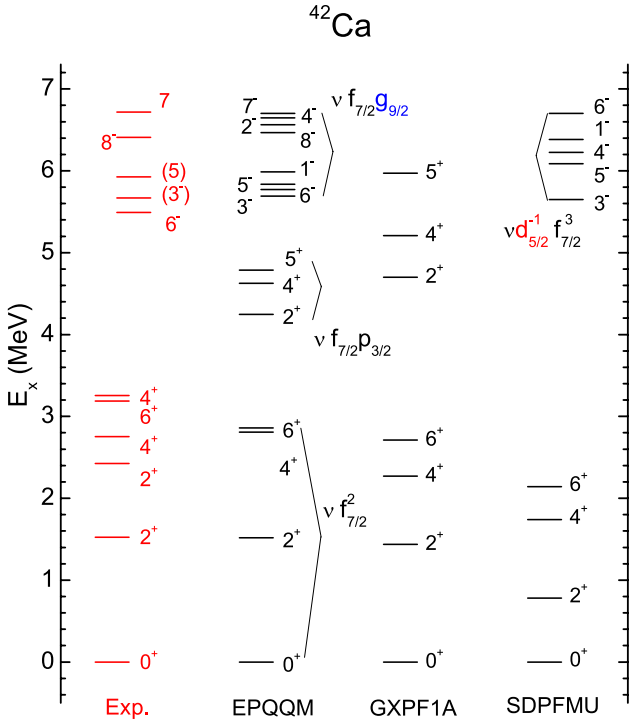

Fig. 1 The experimental energy levels in ^{42}Ca [30], and the theoretical levels calculated by interactions EPQQM, GXPF1A, and SDPFMU

model calculations. The ground state and excited levels 2^+, 4^+, and 6^+ exhibit the same main configuration $\nu f_{7/2}^2$ as suggested by the EPQQM, GXPF1A, and SDPFMU interactions. The second 2^+ and 4^+ levels predominantly feature the configuration $\nu f_{7/2}p_{3/2}$.

Regarding negative parity levels, the 8^- configuration $\nu f_{7/2}g_{9/2}$ closely corresponds to the observed 8^- state at 6.408 MeV. This configuration successfully reproduces the (3^-), (5^-), and 6^- states. The 7^- state at 6.703 MeV is in proximity to the datum at 6.718 MeV, although its parity information remains unconfirmed. The levels 1^-, 2^-, and 4^- are well-predicted in this study. However, the GXPF1A interaction fails to reproduce the negative parity levels in ^{42}Ca due to the absence of cross-shell and intruder orbits in the model space. In contrast, the SDPFMU interaction, which considers the cross-shell proton (neutron) $d_{5/2}$ orbit under $Z = 20$ ($N = 20$), successfully predicts negative levels around 6 MeV with the primary configuration $\nu d^{-1}5/2f^3 7/2$.

The low-lying states of ^{42}Ca can be used to determine the pairing and multipole force strengths in the neutron model space. As shown in Fig. 1, the experimental data in ^{42}Ca are listed and compared with shell model calculations. The ground state and excited levels 2^+, 4^+, and 6^+ are consistently described by the same main configuration

$\nu f_{7/2}^2$ according to three different interactions: EPQQM, GXPF1A, and SDPFMU. There are also small differences in the mixed minor configurations. In the EPQQM model, the ground state 0^+ has approximately 82% of $\nu f_{7/2}^2$ 6.3 % of $\nu p_{3/2}^2$, and 8.3% of $\nu f_{5/2}^2$. The configurations $\nu p_{1/2}^2$ and $\nu g_{9/2}^2$ occupy only about 2%, respectively. In GXPF1A model, the ground state 0^+ has 97 % of $\nu f_{7/2}^2$, and only 1.6 % of $\nu p_{3/2}^2$. In SDPFMU model, the ground state 0^+ has 92 % of $\nu f_{7/2}^2$, and no other configuration more than 1.52%.

In EPQQM, the first 2^+ state has 79.8 % of $\nu f_{7/2}^2$ and 10.4% of $\nu f_{7/2}p_{3/2}$, while it has 96.8% of $\nu f_{7/2}^2$ and 2.8 % of $\nu f_{7/2}p_{3/2}$ by GXPF1A model. The second 2^+ level has 73.7% of configuration $\nu f_{7/2}p_{3/2}$ and 16.8% of $\nu f_{7/2}^2$ in this work, while it has 92.7% of $\nu f_{7/2}p_{3/2}$ in GXPF1A model. The difference increases in the minor configuration of this level, between EPQQM and GXPF1A models. The second 4^+ has 97.1% of $\nu f_{7/2}p_{3/2}$ in EPQQM, while it has 93.2% of $\nu f_{7/2}p_{3/2}$ in GXPF1A. The difference decreases in the second 4^+.

For negative parity level states, the 8^- coupled by $\nu f_{7/2}g_{9/2}$ is very close to the datum 8^- at 6.408 MeV. This configuration has 8 members from the 1^- to 8^- level, effectively reproducing the data of (3^-), (5^-), and 6^- states. The 7^- state at 6.703 MeV is close to the datum 6.718 MeV, which includes unconfirmed parity information. This study successfully predicts the levels 1^-, 2^-, and 4^-. The 8^- level at 6.468MeV has 100 % of $\nu f_{7/2}g_{9/2}$, because only this configuration can produce the $J = 8$ state. In addition to the main configuration $\nu f_{7/2}g_{9/2}$, the 7^- state has a minor configuration of $\nu f_{5/2}g_{9/2}$, only 0.5%. The 6^- (5^-)state has a minor configuration of $\nu p_{3/2}g_{9/2}$, 2.9 (3.93) %. The levels 4^- and 3^- also have a little part of $\nu p_{3/2}g_{9/2}$. The levels 2^- and 1^- are only reproduced by configuration $\nu f_{7/2}g_{9/2}$ in the present model space. For the other two interactions, the GXPF1A is not able to reproduce the negative parity levels in ^{42}Ca owing to the lack of cross-shell and intrusive orbits in the model space. While considering the cross-shell proton (neutron) $d_{5/2}$ orbit under $Z = 20$ ($N = 20$), the SDPFMU provides negative levels at approximately 6 MeV with the main configuration $\nu d_{5/2}^{-1}f_{7/2}^3$.

3.2 ^{42}Ti

The ground state of ^{42}Ti, which is the mirror nucleus of ^{42}Ca, is unstable with a half-life of 211.7 ms (19), as determined from analysis of beta decay and correlated implantations. Levels of ^{42}Ti excite up around 7 MeV with the highest spin $J^\pi = 6^+$. The low-lying states in ^{42}Ti are used to determine the strengths of pairing and multipole forces in the proton model space. In the even–even nucleus of ^{42}

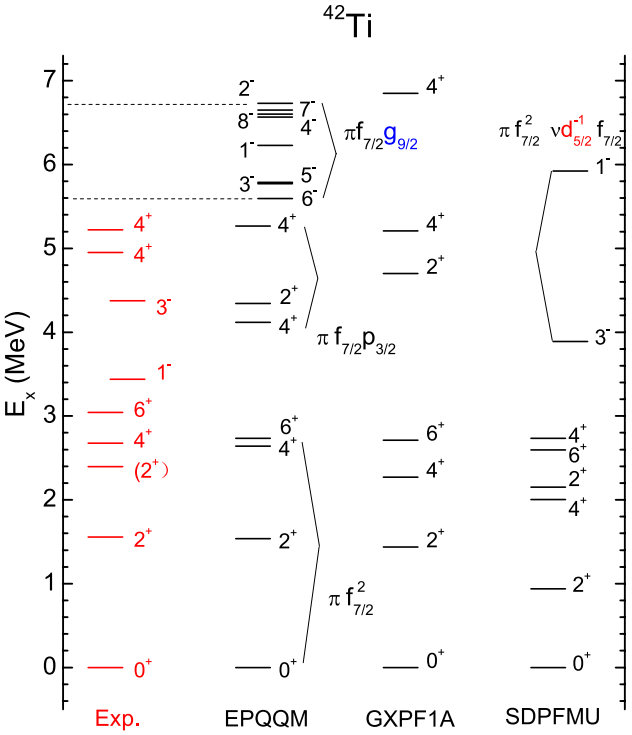

Fig. 2 The calculations and experimental energy levels in ^{42}Ti[30]

Ti, the EPQQM model suggests that the main configuration of the 0^+, 2^+, 4^+, and 6^+ levels is $\pi f_{7/2}^2$ (Fig. 2). In this work, the ground state 0^+ has 81 % of $\pi f_{7/2}^2$, 8.8 % of $\pi f_{5/2}^2$, and 6 % of $\pi p_{3/2}^2$. In GXPF1A model, the ground state has 97 % of $\pi f_{7/2}^2$ and 1.6 % of $\pi p_{3/2}^2$. In SDPFMU model, the ground state has 73.4 % of $\pi f_{7/2}^2$ and 16.3 % of $\pi p_{1/2}^2$. These three models have the same main configuration and only some difference in minor configurations. In the second 2^+ and 4^+ levels, these three interactions show a small difference in configurations. The EPQQM has 78.7 % (94.4 %) configuration $\pi f_{7/2}p_{3/2}$ in the second 2^+ (4^+) levels, while in GXPF1A is 92.7 % (93.2 %) The SDPFMU has 53 % (65 %) of $\pi f_{7/2}p_{3/2}$ in the second 2^+ (4^+) levels, respectively.

In this study, the negative parity levels ranging from 1^- to 8^- coupled by the configuration $\pi f_{7/2}g_{9/2}$ are found to be good predictions, which appear at approximately 6 MeV. There is still no experimental data of negative parity levels in this energy range. The high spin level 8^- at 6.602 MeV is only coupled by the configuration $\pi f_{7/2}g_{9/2}$. The level 7^- at 6.651 MeV has 99.7% of $\pi f_{7/2}g_{9/2}$ and 0.3% of $\pi f_{5/2}g_{9/2}$. The level 6^- at 5.593 MeV has 96.0% of $\pi f_{7/2}g_{9/2}$ and 4.0% of $\pi p_{3/2}g_{9/2}$. The level 5^- (4^-) at 5.789(6.567) MeV has 97.1(95.6)% of $\pi f_{7/2}g_{9/2}$ and 2.6(3.5)% of $\pi p_{3/2}g_{9/2}$. The levels 1^-, 2^-, and 3^- are also coupled by configuration $\pi f_{7/2}g_{9/2}$ completely. Another type of

negative parity levels are coupled by neutron cross-shell excitations from the *sd* shell under $N = 20$. The 1^- and 3^- levels, obtained from the SDPFMU interaction, exhibit a dominant configuration of $\pi f_{7/2}^2 \nu d^{-1} 5/2f7/2$.

When comparing the experimental data of ^{42}Ca and ^{42}Ti, some differences are observed in the low-lying energy levels. For example, the first 2^+, 4^+, and 6^+ levels of ^{42}Ti are slightly higher than those of ^{42}Ca, while the GXPF1A interaction predicts the same energy values. The EPQQM interaction, by incorporating different force strengths for protons and neutrons, effectively captures the distinction between ^{42}Ca and ^{42}Ti. As shown in Table 1, the pairing force strength of $g_{0,pp}(g_{2,pp})$ is 0.450 (0.470), while $g_{0,nn}(g_{2,nn})$ is 0.422 (0.449). This small discrepancy in force strengths can accurately reproduce the energy difference between ^{42}Ca and ^{42}Ti as observed in experiments.

3.3 ^{42}Sc

As an odd–odd nucleus, ^{42}Sc offers a unique opportunity to investigate the correlations between proton and neutron states. The excited states in ^{42}Sc extend up to energies of 13 MeV, with the highest observed spin being $J = 15$. However, at present, the parity information for these states remains unknown. Theoretical calculations suggest that the configurations of low-lying states in ^{42}Sc are formed by coupling the proton and neutron single-particle states appearing in ^{41}Sc and ^{41}Ca (Fig. 3). Shell model calculations predict that the main configuration of the ground state in ^{42}Sc is $\pi f_{7/2} \nu f_{7/2}$ that couples eight states from 0^+ to 7^+. Here, the 0^+ state is taken as the ground state in ^{42}Sc and it matches the experimental data well. The interactions of GXPF1A (Th. 2) and SDPFMU (Th. 3) provide the 7^+ state as the lowest state. The 7^+ level at 0.616 MeV from the level systematics and shell model expectations is a long half-life isomer with an average of 61.7(4)s, which is significantly longer than the ground state 0^+ at 680.79(28) ms [30].

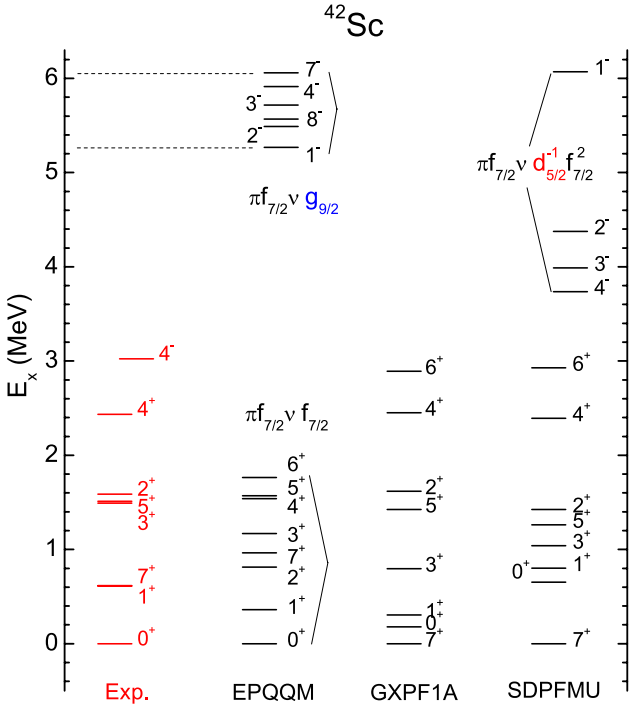

Fig. 3 The calculations and experimental energy levels in ^{42}Sc [30]

In EPQQM model, the ground state 0^+ has 91.4% of configuration $\pi f_{7/2} \nu f_{7/2}$ and 7.7% of configuration $\pi p_{3/2} \nu p_{3/2}$. The first excited state 1^+ at 0.361MeV has 94.0% of configuration $\pi f_{7/2} \nu f_{7/2}$ and 4.6% of configuration $\pi p_{3/2} \nu p_{3/2}$. The level 7^+ at 0.965 MeV is near to the datum 0.616 MeV, which is completely coupled by configuration $\pi f_{7/2} \nu f_{7/2}$. The level 5^+ at 1.570 MeV is close to the datum 1.510 MeV, which has 77.3% of configuration $\pi f_{7/2} \nu f_{7/2}$, 12.6% of configuration $\pi p_{3/2} \nu f_{7/2}$, and 9.9% of configuration $\pi f_{7/2} \nu p_{3/2}$. The level 6^+ is predicted at 1.763 MeV with a main configuration of $\pi f_{7/2} \nu f_{7/2}$. Theoretical calculations based on the three different interactions efficiently fit the experimental data of the observed 1^+, 3^+, and 5^+ states.

As for negative parity levels coupled by the intruder orbit $g_{9/2}$, they lie above 5 MeV with a main configuration $\pi f_{7/2} \nu g_{9/2}$. There is no datum observed in this energy extent. The level 1^- at 5.269MeV is completely coupled by the configuration $\pi f_{7/2} \nu g_{9/2}$. The level 2^- at 5.488MeV has 99.6 % of configuration $\pi f_{7/2} \nu g_{9/2}$. The level 8^- at 5.569MeV is completely coupled by the configuration $\pi f_{7/2} \nu g_{9/2}$. The SDPFMU interaction provides negative parity levels as neutron core excitations around 5 MeV, with the main configuration $\pi f_{7/2} \nu d_{5/2}^{-1} f_{7/2}^2$.

3.4 ^{43}Ti

In this study, the energy levels in ^{43}Ti are examined as an additional test of the current model (Fig. 4). Owing to the presence of an odd number of valence nucleons, the pf shell model space only couples negative parity levels. The positive parity levels can be coupled through intruder orbit $g_{9/2}$ or cross-shell excitations. The ground state $7/2^-$ is well reproduced by all three different models with a main configuration of $\pi f_{7/2}^2 \nu f_{7/2}$, while some difference exists in percentages and minor configurations. In EPQQM, the ground state has 76.9% of configuration $\pi f_{7/2}^2 \nu f_{7/2}$, 6.1% of configuration $\pi f_{5/2}^2 \nu f_{7/2}$, and 5.0% of configuration $\pi p_{3/2}^2 \nu f_{7/2}$. In GXPF1A, the ground state has 86.8% of configuration $\pi f_{7/2}^2 \nu f_{7/2}$, 2.3% of configuration $\pi f_{5/2}^2 \nu p_{1/2}$, and 1.8% of configuration $\pi f_{7/2} p_{3/2} \nu f_{7/2}$. In SDPFMU, the ground state has

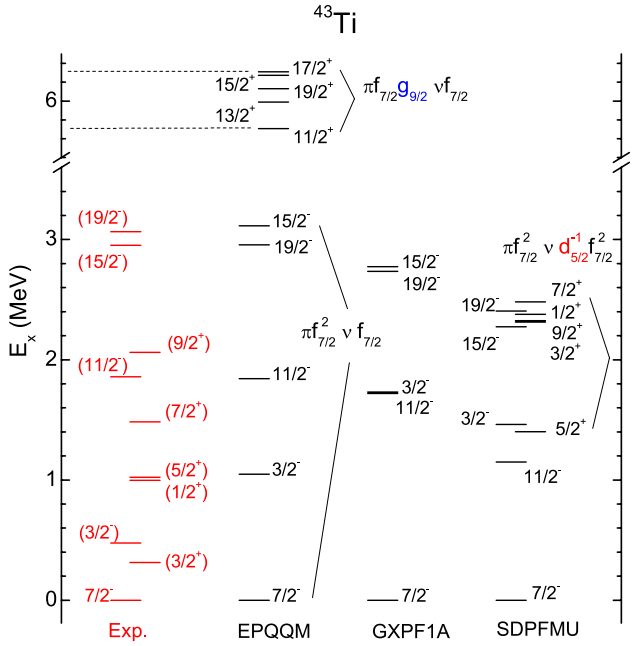

Fig. 4 Calculations and experimental energy levels in ^{43}Ti [30]

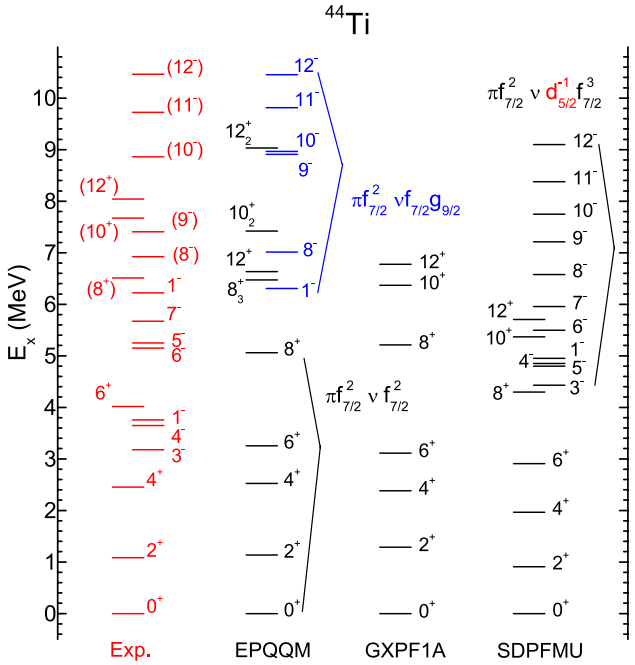

Fig. 5 The calculations and experimental energy levels in ^{44}Ti[30]

79.2% of configuration $\pi f_{7/2}^2 \nu f_{7/2}$, 4.7% of configuration $\pi p_{1/2}^2 \nu f_{1/2}$, and 3.8% of configuration $\pi f_{7/2} p_{3/2} \nu f_{7/2}$.

The state $3/2^-$ has mixed configurations as follows: 27.9% (30.4%) of $\pi f_{7/2}^2 \nu f_{7/2}$, 28.0% (23.9%) of $\pi f_{7/2}^2 \nu p_{3/2}$, and 20.7% (24.1%) $\pi f_{7/2} p_{3/2} \nu f_{7/2}$ by EPQQM (GXPF1A) model. The SDPFMU model has some difference in this state's configurations, which has a major part of 50.1% $\pi f_{7/2} f_{5/2} \nu f_{7/2}$, and a minor part of 24.6% of $\pi f_{7/2}^2 \nu f_{7/2}$. In EPQQM, the level $11/2^-$ at 1.842 MeV is very close to the datum 1.858 MeV, with a difference factor 0.991. Its state has 70.7% of configuration $\pi f_{7/2}^2 \nu f_{7/2}$ and 16.7% of configuration $\pi f_{7/2} p_{3/2} \nu f_{7/2}$. The levels $15/2^-$, and $19/2^-$ also have a main configuration $\pi f_{7/2}^2 \nu f_{7/2}$.

The positive parity states around 6 MeV are coupled by two main configurations $\pi f_{7/2} g_{9/2} \nu f_{7/2}$ and $\pi f_{7/2}^2 \nu g_{9/2}$. The level $11/2^+$ at 5.708 MeV has 95.1% of $\pi f_{7/2} g_{9/2} \nu f_{7/2}$. The level $13/2^+$ at 5.990 MeV has 91.4% of $\pi f_{7/2} g_{9/2} \nu f_{7/2}$. The levels $15/2^+$, $17/2^+$, and $19/2^+$ have about 95 % of $\pi f_{7/2} g_{9/2} \nu f_{7/2}$. Except the level $9/2^+$, the states from $1/2^+$ to $21/2^+$ around 6 MeV are all coupled by this configuration. The level $9/2^+$ at 4.923 MeV belongs to configuration $\pi f_{7/2}^2 \nu g_{9/2}$. The interaction SDPFMU produces positive parity states near 2 MeV, which are coupled by neutron core excitations of configuration $\pi f_{7/2}^2 \nu d_{5/2}^{-1} f_{7/2}^2$.

3.5 ^{44}Ti

As a self-conjugated nucleus, ^{44}Ti is a benchmark for shell model calculations in the northeast of the doubly magic nucleus ^{40}Ca. With two protons and two neutrons as valence nucleons, the nucleus ^{44}Ti has more complicated and high energy states. The excited states in ^{44}Ti reach up to 16 MeV, and the highest spin is 15 with negative parity information. For the positive parity levels shown in Fig. 5, the 0^+, 2^+, 4^+, 6^+, and 12^+ levels have a main configuration $\pi f_{7/2}^2 \nu f_{7/2}^2$ according to the three different interactions, while some difference is found in percentages and minor configurations.

In the EPQQM model, the ground state 0^+ of ^{42}Ca is composed of 56.7% $\pi f_{7/2}^2 \nu f_{7/2}^2$ configuration. On the other hand, in the GXPF1A and SDPFMU models, the ground state 0^+ consists of 70.4% and 78.5% $\pi f_{7/2}^2 \nu f_{7/2}^2$ configurations, respectively.

Similarly, for the 2^+ state, the EPQQM model predicts a 50.0% $\pi f_{7/2}^2 \nu f_{7/2}^2$ configuration, while the GXPF1A and SDPFMU models assign 64.1% and 79.1% $\pi f_{7/2}^2 \nu f_{7/2}^2$ configurations, respectively.

In the case of the 4^+ state, the EPQQM model predicts a 54.8% $\pi f_{7/2}^2 \nu f_{7/2}^2$ configuration, whereas the GXPF1A and SDPFMU models assign 56.7% and 74.6% $\pi f_{7/2}^2 \nu f_{7/2}^2$ configurations, respectively.

Overall, the configurations in the GXPF1A and SDPFMU models tend to be more concentrated in the states of ^{42}Ca

compared to the EPQQM model, indicating a stronger dominance of the $\pi f_{7/2}^2 \nu f_{7/2}^2$ configuration in these models.

In this study, the calculated energy levels from 0^+ to 6^+ are found to be in good agreement with the experimental data, indicating a successful reproduction of these states by the model used. Furthermore, when considering the high spin levels 8^+, 10^+, and 12^+, the EPQQM model yields better results compared to the GXPF1A and SDPFMU models.

With even-valence nucleons, only positive parity levels can be coupled in the model space of the pf shell. The negative parity levels are from cross-shell excitations or are coupled by the intruder orbit $g_{9/2}$. As neutron core excitations, the SDPFMU interactions provide negative parity states from 1^- to 12^- in the energy range from 4 to 9 MeV. Their main configuration is $\pi f_{7/2}^2 \nu d_{5/2}^{-1} f_{7/2}^3$, while the 5^- to 9^- states fit the corresponding experimental data well.

For the negative parity states coupled by the intruder orbit $g_{9/2}$, the EPQQM model reproduces very well the data (1^-), (8^-), (10^-), (11^-), and (12^-), which has a main configuration $\pi f_{7/2}^2 \nu f_{7/2} g_{9/2}$. This good fit, coupled with intruder orbit $g_{9/2}$ in nuclei ^{42}Sc, ^{42}Ti, and ^{43}Ti confirms our predictions. The level 1^- at 6.309 MeV has 77.5 % of configuration $\pi f_{7/2}^2 \nu f_{7/2} g_{9/2}$, which is very close to datum 1^- at 6.220 MeV. The level 8^- at 7.012 MeV has 79.5 % of configuration $\pi f_{7/2}^2 \nu f_{7/2} g_{9/2}$, with a difference factor 1.013 to the datum (8^-) at 6.924 MeV. The level 10^- at 8.968 MeV has a difference factor 1.012 by comparing with datum (10^-) at 8.861 MeV. The level 11^- at 9.815 MeV has 86.8 % of configuration $\pi f_{7/2}^2 \nu f_{7/2} g_{9/2}$, with a difference factor 1.009 to its corresponding datum (11^-) at 9.723 MeV. The level 12^- at 10.455 MeV has 86.8 % of configuration $\pi f_{7/2}^2 \nu f_{7/2} g_{9/2}$, with a difference factor 0.9992 to its corresponding datum (12^-) at 10.463 MeV. The shell model with EPQQM interaction works very accurately even at about 10 MeV.

4 Summary

In this work, we have developed a new interaction with the *pf* shell and the intruder orbit $g_{9/2}$, and studied the energy levels of nuclei ^{42}Ca, ^{42}Sc, and $^{42-44}$Ti near the doubly magic nucleus ^{40}Ca. The main conclusions of the present study are as follows:

(1) For ^{42}Ca, ^{42}Sc, and ^{42}Ti, the low-lying levels in positive parity have been well reproduced, and negative parity levels have been predicted to be coupled by the intruder orbit $g_{9/2}$. In ^{42}Ca (^{42}Ti), the negative parity members of $\nu f_{7/2} g_{9/2}$ ($\pi f_{7/2} g_{9/2}$) are predicted around 6 MeV, while in ^{42}Sc, the negative parity levels coupled by the configuration $\pi f_{7/2} \nu g_{9/2}$ are predicted to be above 5 MeV.

(2) In the case of ^{43}Ti, the theoretical calculations successfully reproduce the negative parity levels. Additionally, the positive parity configurations, specifically $\pi f_{7/2} g_{9/2} \nu f_{7/2}$, which are coupled by the intruder orbit $g_{9/2}$, are predicted to appear at approximately 6 MeV

(3) In the case of ^{44}Ti, all three different interactions used in the study successfully reproduce the energy levels of the first 2^+, 4^+, and 6^+ states. Specifically, the EPQQM interaction shows excellent agreement with the experimental data for the (1^-), (8^-), (10^-), (11^-), and (12^-) states, which have a dominant configuration of $\pi f_{7/2}^2 \nu f_{7/2} g_{9/2}$. This successful reproduction of the data further confirms the accuracy of the predictions made for the levels of ^{42}Sc, ^{42}Ti, and ^{43}Ti, which are coupled by the intruder orbit $g_{9/2}$.

(4) It is necessary to consider the intruder orbit $g_{9/2}$ when studying the high energy states in nuclei near the doubly magic nucleus ^{40}Ca. The present work provides a new, useful interaction for further experimental and theoretical research in this region, such as, band mixing in this region.

Author contributions All authors contributed to the study conception and design. Material preparation and data collection and analysis were performed by Jin-Zhong Han, Shuai Xu, Amir Jalili, and Han-Kui Wang. The first draft of the manuscript was written by Han-Kui Wang and all authors commented on previous versions of the manuscript. All authors read and approved the final manuscript.

Data availability The data that support the findings of this study are openly available in Science Data Bank at https://doi.org/10.57760/sciencedb.08187 and https://cstr.cn/31253.11.sciencedb.08187.

Conflict of interest The authors declare that they have no competing interests.

References

1. W.R. Dixon, R.S. Storey, J.J. Simpson, Lifetimes of ^{44}Ti levels. Nucl. Phys. A **202**, 579 (1973). https://doi.org/10.1016/0375-9474(73)90644-1
2. J.J. Simpson, W.R. Dixon, R.S. Storey, Evidence for rotational bands in ^{44}Ti. Phys. Rev. Lett. **31**, 946 (1973). https://doi.org/10.1103/PhysRevLett.31.946
3. W.R. Dixon, R.S. Storey, J.J. Simpson, Levels of ^{44}Ti from the ^{40}Ca(α,γ) ^{44}Ti reaction. Phys. Rev. C **15**, 1896 (1977). https://doi.org/10.1103/PhysRevC.15.1896
4. J.W. Olness, J.J. Kolata, E.K. Warburton, High-spin states in ^{44}Ti and ^{44}Sc*. Phys. Rev. C **10**, 1663 (1974). https://doi.org/10.1103/PhysRevC.10.1663
5. C. Michelagnoli, C.A. Ur, E. Farnea et al., Lifetime measurement in the $N = Z$ nucleus ^{44}Ti*. Acta Phys. Pol., B **42**, 825 (2011). https://doi.org/10.5506/APhysPolB.42.825
6. K. Arnswald, T. Braunroth, M. Seidlitz et al., Enhanced collectivity along the $N = Z$ line: Lifetime measurements in ^{44}Ti, ^{48}Cr, and

^{52}Fe. Phys. Lett. B **772**, 599–606 (2017). https://doi.org/10.1016/j.physletb.2017.07.032
7. K. Arnswald, P. Reiter, A. Blazhev et al., Lifetime measurements in ^{44}Ti. Phys. Rev. C **102**, 054302 (2020). https://doi.org/10.1103/PhysRevC.102.054302
8. L. Zhou, S.M. Wang, D.Q. Fang et al., Recent progress in two-proton radioactivity. Nucl. Sci. Tech. **33**, 105 (2022). https://doi.org/10.1007/s41365-022-01091-1
9. X. Zhou, M. Wang, Y.H. Zhang et al., Charge resolution in the isochronous mass spectrometry and the mass of ^{51}Co. Nucl. Sci. Tech. **32**, 37 (2021). https://doi.org/10.1007/s41365-021-00876-0
10. X.B. Wei, H.L. Wei, Y.T. Wang et al., Multiple-models predictions for drip line nuclides in projectile fragmentation of ^{40,48}Ca, ^{58,64}Ni, and ^{78,86}Kr at 140 MeV/u. Nucl. Sci. Tech. **33**, 155 (2022). https://doi.org/10.1007/s41365-022-01137-4
11. Y.F. Gao, B.S. Cai, C.X. Yuan et al., Investigation of β^- decay half-life and delayed neutron emission with uncertainty analysis. Nucl. Sci. Tech. **34**, 9 (2023). https://doi.org/10.1007/s41365-022-01153-4
12. A.A. Raduta, L. Zamick, E. Moya de Guerra et al., Description of single and double analog states in the $f_{7/2}$ shell: The Ti isotopes. Phys. Rev. C **68**, 044317 (2003). https://doi.org/10.1103/PhysRevC.68.044317
13. A. Juodagalvis, I. Ragnarsson, S. Aberg, Cranked Nilsson-Strutinsky vs the spherical shell model: A comparative study of pf-shell nuclei. Phys. Rev. C **73**, 044327 (2006). https://doi.org/10.1103/PhysRevC.73.044327
14. Y. Utsuno, T. Otsuka, B. Alex Brown et al., Shape transitions in exotic Si and S isotopes and tensor-force-driven Jahn-Teller effect. Phys. Rev. C **86**, 051301 (2012). https://doi.org/10.1103/PhysRevC.86.051301
15. B.A. Brown, B.H. Wildenthal, Status of the nuclear shell model. Annu. Rev. Nucl. Part. Sci. **38**, 29 (1988). https://doi.org/10.1146/annurev.ns.38.120188.000333
16. M. Honma, T. Otsuka, B.A. Brown et al., Shell-model description of neutron-rich pf-shell nuclei with a new effective interaction GXPF1. Eur. Phys. J. A **25**, 499 (2005). https://doi.org/10.1140/epjad/i2005-06-032-2
17. Y. Utsuno, T. Otsuka, T. Mizusaki et al., Varying shell gap and deformation in N~20 unstable nuclei studied by the Monte Carlo shell model. Phys. Rev. C **60**, 054315 (1999). https://doi.org/10.1103/PhysRevC.60.054315
18. A. Poves, A. Zuker, Theoretical spectroscopy and the fp shell. Phys. Rep. **70**, 235 (1981). https://doi.org/10.1016/0370-1573(81)90153-8
19. M. Hasegawa, K. Kaneko, S. Tazaki, Improvement of the extended P + QQ interaction by modifying the monopole field. Nucl. Phys. A **688**, 765 (2001). https://doi.org/10.1016/S0375-9474(00)00602-3
20. K. Kaneko, M. Hasegawa, T. Mizusaki, Quadrupole and octupole softness in the $N = Z$ nucleus ^{64}Ge. Phys. Rev. C **66**, 051306(R) (2002). https://doi.org/10.1103/PhysRevC.66.051306
21. K. Kaneko, Y. Sun, M. Hasegawa et al., Shell model study of single-particle and collective structure in neutron-rich Cr isotopes. Phys. Rev. C **78**, 064312 (2008). https://doi.org/10.1103/PhysRevC.78.064312
22. K. Kaneko, Y. Sun, T. Mizusaki et al., Shell-model study for neutron-rich sd-shell nuclei. Phys. Rev. C **83**, 014320 (2011). https://doi.org/10.1103/PhysRevC.83.014320
23. H.K. Wang, S.K. Ghorui, Z.Q. Chen et al., Analysis of low-lying states, neutron-core excitations, and electromagnetic transitions in tellurium isotopes $^{130-134}$Te. Phys. Rev. C **102**, 054316 (2020). https://doi.org/10.1103/PhysRevC.102.054316
24. H.K. Wang, S.K. Ghorui, K. Kaneko et al., Large-scale shell-model study for excitations across the neutron $N = 82$ shell gap in $^{131-133}$Sb. Phys. Rev. C **96**, 054313 (2017). https://doi.org/10.1103/PhysRevC.96.054313
25. H.K. Wang, Y. Sun, H. Jin et al., Structure analysis for hole-nuclei close to ^{132}Sn by a large-scale shell-model calculation. Phys. Rev. C **88**, 054310 (2013). https://doi.org/10.1103/PhysRevC.88.054310
26. H.K. Wang, K. Kaneko, Y. Sun, Isomerism and persistence of the $N = 82$ shell closure in the neutron-rich ^{132}Sn region. Phys. Rev. C **89**, 064311 (2014). https://doi.org/10.1103/PhysRevC.89.064311
27. H.K. Wang, K. Kaneko, Y. Sun et al., Monopole effects, isomeric states, and cross-shell excitations in the $A = 129$ hole nuclei near ^{132}Sn. Phys. Rev. C **95**, 011304 (2017). https://doi.org/10.1103/PhysRevC.103.024317
28. A.J. Majarshin, Y.A. Luo, F. Pan et al., Nuclear structure and band mixing in ^{194}Pt. Phys. Rev. C **103**, 024317 (2021). https://doi.org/10.1103/PhysRevC.103.024317
29. A.J. Majarshin, Y.A. Luo, F. Pan et al., Structure of rotational bands in ^{109}Rh. Phys. Rev. C **104**, 014321 (2021). https://doi.org/10.1103/PhysRevC.104.014321
30. http://www.nndc.bnl.gov/ensdf/
31. B.A. Brown, W.D.M. Rae, The shell-model code NuShellX@MSU. Nucl. Data Sheets **120**, 115 (2014). https://doi.org/10.1016/j.nds.2014.07.022
32. Y.Z. Ma, L. Coraggio, L.D. Augelis et al., Contribution of chiral three-body forces to the monopole component of the effective shell-model Hamiltonian. Phys. Rev. C **100**, 034324 (2019). https://doi.org/10.1103/PhysRevC.100.034324
33. S.R. Stroberg, H. Hergert, S.K. Bogner et al., Nonempirical interactions for the nuclear shell model: An update. Annu. Rev. Nucl. Part. Sci. **69**, 307 (2017). https://doi.org/10.1146/annurev-nucl-101917-021120
34. A.P. Zuker, Three-body monopole corrections to realistic interactions. Phys. Rev. Lett. **90**, 042502 (2003). https://doi.org/10.1103/PhysRevLett.90.042502
35. H.K. Wang, Z.H. Li, Y.B. Wang et al., High-spin levels, β-decay and monopole effects in $A = 128$ hole nuclei near ^{132}Sn. Phys. Lett. B **833**, 137337 (2022). https://doi.org/10.1016/j.physletb.2022.137337
36. R.F. Takaharu Otsuka, T. Suzuki, H. Grawe et al., Evolution of nuclear shells due to the tensor force. Phys. Rev. Lett. **95**, 232502 (2005). https://doi.org/10.1103/PhysRevLett.95.232502
37. H.K. Wang, Z.Q. Chen, H. Jin et al., Ground state inversions in hole nuclei near 132Sn driven by the monopole interaction. Phys. Rev. C **104**, 014301 (2021). https://doi.org/10.1103/PhysRevC.104.014301